water

MDPI

Article

Investigating Impacts of Climate Change on Runoff from the Qinhuai River by Using the SWAT Model and CMIP6 Scenarios

Jinqiu Sun [1,2,3], Haofang Yan [4], Zhenxin Bao [1,2,3] and Guoqing Wang [1,2,3,*]

1 State Key Laboratory of Hydrology-Water Resources and Hydraulic Engineering, Nanjing Hydraulic Research Institute, Nanjing 210029, China; jqsun@nhri.cn (J.S.); zxbao@nhri.cn (Z.B.)
2 Yangtze Institute for Conservation and Development, Nanjing 210098, China
3 Research Center for Climate Change, Ministry of Water Resources, Nanjing 210029, China
4 Research Centre of Fluid Machinery Engineering and Technology, Jiangsu University, Zhenjiang 212013, China; 1000004265@ujs.edu.cn
* Correspondence: gqwang@nhri.cn

Abstract: This paper looks at regional water security in eastern China in the context of global climate change. The response of runoff to climate change in the Qinhuai River Basin, a typical river in eastern China, was quantitatively investigated by using the Soil and Water Assessment Tool (SWAT) model and the ensemble projection of multiple general circulation models (GCMs) under three different shared socioeconomic pathways (SSPs) emission scenarios. The results show that the calibrated SWAT model is applicable to the Qinhuai River Basin and can accurately characterize the runoff process at daily and monthly scales with the Nash–Sutcliffe efficiency coefficients (NSE), correlation coefficients (R), and the Kling–Gupta efficiency (KGE) in calibration and validation periods being above 0.75 and relative errors (RE) are ±3.5%. In comparison to the baseline of 1980–2015, the mean annual precipitation in the future period (2025–2060) under the three emission scenarios of SSP1-2.6, SSP2-4.5, and SSP5-8.5 will probably increase by 5.64%, 2.60%, and 6.68% respectively. Correspondingly, the multiple-year average of daily maximum and minimum air temperatures are projected to rise by 1.6–2.1 °C and 1.4–2.0 °C, respectively, in 2025–2060. As a result of climate change, the average annual runoff will increase by 16.24%, 8.84%, and 17.96%, respectively, in the period of 2025–2060 under the three SSPs scenarios. The increase in runoff in the future will provide sufficient water supply to support socioeconomic development. However, increases in both rainfall and runoff also imply an increased risk of flooding due to climate change. Therefore, the impact of climate change on flooding in the Qinhuai River Basin should be fully considered in the planning of flood control and the basin's development.

Keywords: climate change; CMIP6; hydrological response; runoff simulation; SWAT model; the Qinhuai River Basin

check for updates

Citation: Sun, J.; Yan, H.; Bao, Z.; Wang, G. Investigating Impacts of Climate Change on Runoff from the Qinhuai River by Using the SWAT Model and CMIP6 Scenarios. *Water* **2022**, *14*, 1778. https://doi.org/10.3390/w14111778

Academic Editor: Athanasios Loukas

Received: 6 April 2022
Accepted: 30 May 2022
Published: 1 June 2022

1. Introduction

Global climate change is one of the dominant factors affecting hydrological cycles [1], with the water–heat combination change of precipitation and air temperature having a particularly far-reaching impact on runoff [2]. According to a series of reports from the Intergovernmental Panel on Climate Change (IPCC), the issue of global temperature rise is becoming increasingly prominent [3], not only through significant increases in the intensity of extreme precipitation in many regions of the world, especially in parts of southern China, but also in changes to the hydrological cycle rate and runoff formation process in these areas [4,5]. It will continue to play a role in the next 50 or 100 years [6], disturbing the eco-hydrological cycle of the basin. In the context of global warming, rainfall as well as rainfall intensity will be changed, which will change runoff and flood by altering the hydrological cycle. As one of the basic links of the water cycle, runoff is an important breakthrough point for a scientific understanding of the water cycle process and a comprehensive understanding of the characteristics of water resources. Therefore, it is particularly important to deeply and systematically carry out distributed watershed hydrological simulation and model parameter sensitivity analysis, and to explore the response mechanism of watershed runoff under future climate change scenarios.

The Qinhuai River is located in Jiangsu province and is known as "the mother river of Nanjing". Previous studies of the Qinhuai River Basin have mostly focused on the intensification of flood risks caused by rapid urbanization [7,8]. For instance, Wang et al. [9] compared and analyzed the temporary and spatial variation of the water surface ratio and its decisive factors between watershed and urban areas based on the K-mean Clustering Water Index Method and pointed out that human factors are the main driving factors of water surface change. Qin et al. [10] evaluated land use/cover change (LUCC) through the construction of the Decision Tree model with the help of the Surface Energy Balance Algorithm for Land (SEBAL) model. The results showed that significant changes of LUCC transformed paddy fields and dryland into impervious surfaces in large areas, resulting in a downward trend in daily evapotranspiration at the basin scale over the four seasons. Yang et al. [11], Gao et al. [12], and Song et al. [13] also analyzed the influence of the change in underlying surface and drainage capacity of the Qinhuai River Basin on the rainstorm flood process, and urban waterlogging risk changes in the context of high-speed urbanization by coupling MIKE11 and MIKE21 model and using the Hydrologic Engineering Center's Hydrologic Modeling System (HEC-HMS) model. At present, there are few studies on the impact of climate change on hydrological processes in the Qinhuai River Basin.

The response of runoff to global climate change has been extensively investigated by using multiple methods [14,15]. These methods are the statistical analysis method [16,17], the watershed contrast test [18], and the hydrological modeling method [19,20]. The distributed hydrological model has been widely used because it considers both the spatial heterogeneity of the watershed and the physical process of the hydrological cycle [21]. The SWAT model in the distributed model comprehensively considers many factors, such as soil, vegetation, surface water, and groundwater, which are affected by climate change and human activities. With the advantages of high computational efficiency, the ability to simulate long-term continuous hydrological processes and flexibility in application, this model has become an indispensable tool in the process of water resources conservation and management and has been widely used in the simulation of the hydrological cycle and the prediction of the hydrological effects of climate change at a watershed scale at home and abroad [22]. Wang et al. [23] expounded the principle, structure, and application of the SWAT model. In addition, the SWAT model was used to study the Lancang-Mekong River Basin [24], the Zishui Basin [25], and the Vistula and Odra River Basins [26].

In recent years, atmospheric models have also been further developed, which provides a new opportunity to study the hydrological effects of climate change on regional scale. In this study, six global climate models in the Coupled Model Intercomparison Project Phase 6 (CMIP6)—BCCCSM2-MR, MRI-ESM2-0, GFDL-ESM4, CanESM5, INM-CM5-0, and MIROC6—were selected based on their spatial resolution, and three SSP emission scenarios of SSP1-2.6, SSP2-4.5, and SSP5-8.5 were chosen to reproduce future discharge. Previous studies have confirmed that the six selected CMIP6 climate models have good applicability in China [27–29]. Although GCMs model for future meteorological elements has the strong ability of extensional forecast, the spatial resolution of the model itself is low. If the climate model is directly applied to the study of small-scale regional climate change response, the spatial differences in small-scale regions may be ignored. Therefore, the problem of downscaling and bias correction must be considered when using GCMs to predict regional climate change in small watersheds. The downscaling method can transform the results of large-scale and low-resolution GCMs simulation into small-scale and high-resolution regional climate information, to effectively solve the problem of scale mismatch of climate models [30,31]. Among all the different downscaling methods, the statistical downscaling approach such as Inverse Distance Weighting (IDW) is effective and simple in terms of principle and calculation and consistent with the first law of geography [32]; it has been commonly used in hydrology. This method has high requirements for the distribution and density of meteorological stations and is suitable for areas with large density and the small topographic relief of meteorological stations; the observation data of adjacent rainfall stations must have a positive spatial correlation [33]. By downscaling, the temporal and spatial resolution of GCMs in the study of watershed climate characteristics has been improved. After that, it is also necessary to correct the deviation of the data to ensure that it matches the observed data, to further improve the data accuracy. A daily bias correction (DBC) approach is developed by Chen et al. [34,35], which can correct biases of precipitation frequency and intensity simultaneously. This method is a hybrid method that combines the daily transition (DT) method and the local strength scale (LOCI) method, and its good applicability has been widely verified in China [36].

On this basis, the method of combining watershed-scale hydrological models such as SWAT with the output of GCMs to assess the impact of climate change on hydrological processes has been more and more widely used. In previous studies, the method of coupling the SWAT model with global climate models has been validated and applied to some river basins to predict the impact of climate change in the future. He et al. [37] quantitatively simulated the runoff response of the Luo River Basin to climate change by using the SWAT-distributed hydrological model based on future climate scenarios and the land use produced by the CA-Markov model. They found that the change of runoff was positively correlated with the change in precipitation and negatively correlated with the change in temperature. They also found that the influence of land use and climate change on runoff shows a non-linear synergistic effect. Clina et al. [38] combined downscaled general circulation models for three Representative Concentration Pathways (RCPs) in CMIP5 to assess the impacts on discharge regulation and water supply in the Laguna del Sauce catchment. Zhao et al. [39] investigated the variation of hydrological drought in the Weihe River Basin by using three GCMs in two RCP emission scenarios, and the SWAT hydrological model. Tian et al. [40] used two global climate models provided by the CMIP5 and CA-Markov model and combined them with the SWAT model to quantitatively evaluate the impact of climate change and LUCC on runoff. Cheng [41] applied the SWAT model to examine the impact of LUCC and climate change on runoff in the Yuan River Basin in different scenarios. This study clearly illustrated the dominant role of climate change in runoff changes and found that the decrease in runoff was caused by the increase in temperature and decrease in precipitation. The CMIP program has developed to the sixth generation so far, and each update has made the simulated data closer to the real climate change by reviewing past experience and using new technologies. Most of the above studies used CMIP5 model projections, but few used the recently released CMIP6 model projections to evaluate hydrological changes.

Therefore, the target of this study is to use the SWAT model and the available six global climate models provided by the CMIP6 for downscaling and bias correction under three future climate scenarios—SSP1-2.6, SSP2-4.5, and SSP5-8.5—to qualitatively analyze the extent of future climate change and its impact on runoff and to assess the flood risk in the Qinhuai River Basin. This study can provide basic information and scientific evidence for water resources management in the Qinhuai River Basin amid climate change. It is of great theoretical value and practical significance for mastering the mechanism of river basin water cycles, regulating and distributing water resources reasonably, and managing water resources comprehensively.

2. Data and Methodology

2.1. Study Area

The Qinhuai River Basin is situated in southwest Jiangsu province, China (Figure 1). It is located between 31°34′ to 32°10′ North latitude and 118°39′ to 119°19′ East longitude. The basin covers an area of approximately 2631 km^2, with an elevation cram range of −43 to 416 m (Figure 2a). It is a double outlet river basin, with the water source in the South originating from the Jurong River in Baohua Mountain, Jurong, and the water source in the north deriving from the Lishui River in Donglu Mountain, Nanjing. The two rivers converge to the main stream of the Qinhuai in the northwest village of Jiangning district, Nanjing, divert in Dongshan township, and join the Yangtze River at Wudingmen Sluice and Qinhuai River New Sluice in the northwest corner of the river basin. The topography is a complete, fan-shaped structural basin, with the central part a plain surrounded by hills and accounting for 78% of the total area. The subtropical monsoon climate of the study area has four distinct seasons, with abundant rainfall and sufficient sunshine. The multi-year average annual precipitation over the basin is almost 1056 mm, while the average annual temperature is about 15 °C. The land use of the basin is mainly agricultural land, followed by urban commercial land and Forest. The Sankey diagram (Figure 3) shows that the change of land use in the basin from 1980 to 2015 was mainly from cultivated land to residential area, which changed by 240 square kilometers, followed by from cultivated land to forest land, which changed by 22 square kilometers. This indicates that land use change in the study catchment is mainly induced by human activities, such as urbanization, and change in agriculture development, etc.

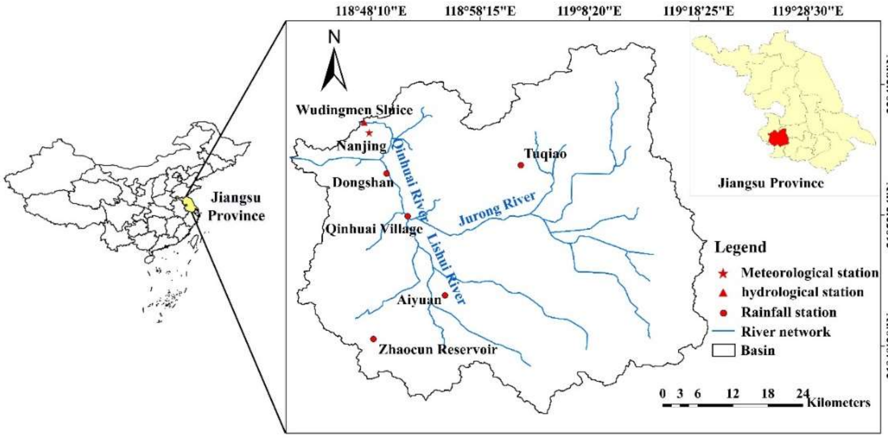

Figure 1. The geographical location of the river network and stations in the Qinhuai River Basin.

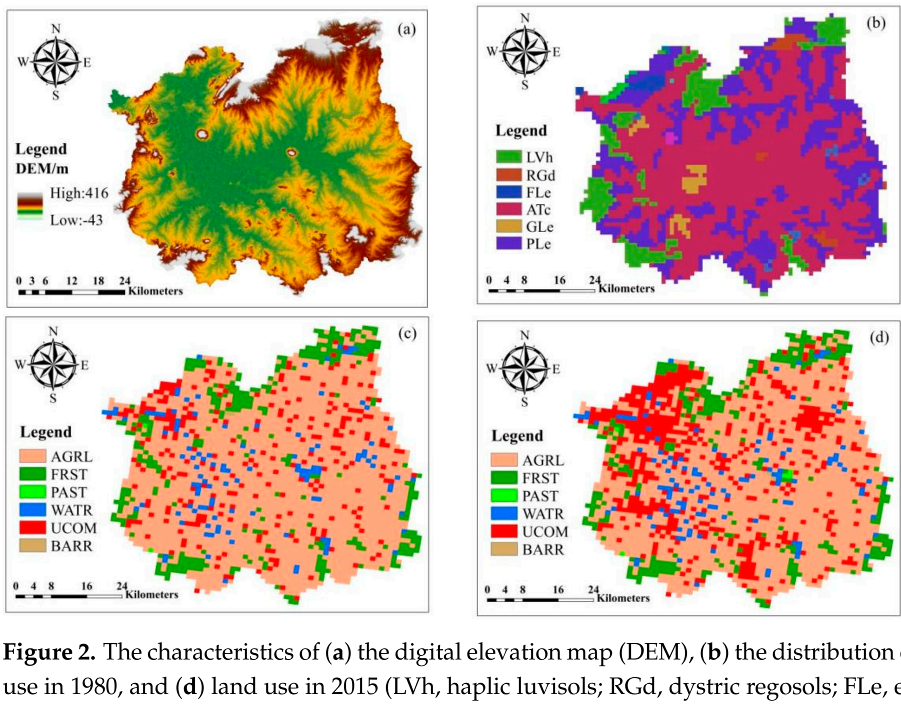

Figure 2. The characteristics of (**a**) the digital elevation map (DEM), (**b**) the distribution of soil, (**c**) land use in 1980, and (**d**) land use in 2015 (LVh, haplic luvisols; RGd, dystric regosols; FLe, eutric fluvisols; ATc, cumulic anthrosols; GLe, eutric gleysols; PLe, eutric planosols; AGRL, agricultural land; FRST, forest; PAST, pasture; WATR, water; UCOM, urban commercial land; and BARR, barren land).

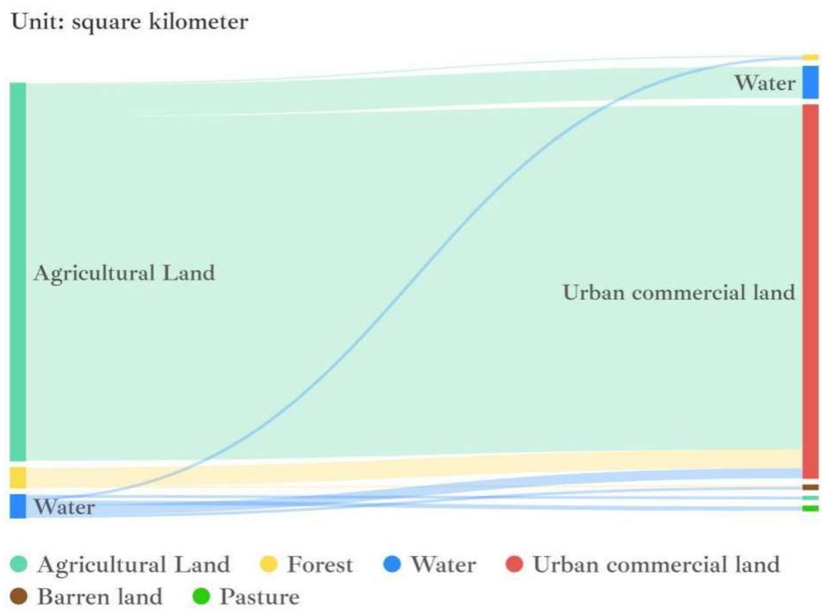

Figure 3. The land use changes in the Qinhuai River Basin from 1980 to 2015.

2.2. SWAT Model

2.2.1. Principle and Development of Model

The Soil and Water Assessment Tool (SWAT) [42] is a public-domain-distributed hydrological model developed by the Agricultural Research Service of the United States Department of Agriculture (USDA-ARS) in 1994. It is a physics-based model that combines the Simulator for Water Resources in Rural Basins (SWRRB) model and the Routing Outputs to Outlet (ROTO) model organically [43]. Since its successful development, the model has been improved several times in more than 30 years and has made great progress in the research depth and application fields. This study was carried out by using the model version of SWAT2012, which is a version with more accurate simulation results by constantly adding new modules, modifying calculation methods, and increasing the scope of application [44]. It takes the day as the time step, simulates the continuous time series, and uses the discretization method to describe the spatial differences of hydrological elements and other parameters in the basin. The hydrological process simulated by the SWAT model can be divided into the runoff generation and overland flow concentration phase and the river confluence phase. In the model, the basin is first divided into multiple sub-basins, and on this basis, the sub-basins are then divided into multiple hydrological response units (HRUs) for simulation operation. In this study, the Qinhuai River Basin is divided into 51 sub-basins and 1582 HRUs.

The model can be used to simulate the changes of discharge under current conditions and under changing underlying surface or meteorological conditions. The operational basis of the model is the water balance equation [45]:

$$SW_t = SW_0 + \sum_{i=1}^{t}\left(R_{day} - Q_{surf} - E_a - w_{seep} - Q_{gw}\right) \quad (1)$$

where SW_0 (mm) is initial soil moisture content, SW_t (mm) is final soil moisture content, R_{day} (mm) is the precipitation at day i, Q_{surf} (mm) is the surface runoff at day i, E_a (mm) is the evapotranspiration at day i, w_{seep} (mm) is the soil flow depth on day i, Q_{gw} (mm) is the groundwater runoff depth on day i, and t (d) is time [46].

2.2.2. Evaluation Indices of Model Applicability

Based on previous studies [40,47–49], the Nash–Sutcliffe efficiency coefficients (NSE), the correlation coefficients (R), the relative error (RE), and the Kling–Gupta efficiency

(KGE) in calibration and validation periods are selected to evaluate the applicability of the model. R is used to evaluate the degree of coincidence between the measured value and the observed value. The closer the R value is to 1, the greater the goodness of fit. If R equals 1, it proves that the two data have sequences that are exactly the same. The relative error can evaluate the deviation between the simulated value and the observed value. The closer the RE value is to 0, the closer the two values are. The Nash efficiency coefficient is also an important standard to measure the simulation effect. The closer the NSE value gets to 1, the closer the simulation results are to the measured values. In general, when $0.75 < \text{NSE} \leq 1$, the simulation consequence is considered to be excellent. The simulation result is considered relatively good when $0.65 \leq \text{NSE} < 0.75$. When $0.5 < \text{NSE} \leq 0.65$, the outcome of the simulation is considered acceptable. The result is considered unacceptable when $\text{NSE} \leq 0.5$ [47]. KGE can pay attention to the R, mean value difference, and standard deviation between the simulated and observed values at the same time. Thus, it can better evaluate the performance of the model. When KGE > 0.7, the model is considered credible. The simulation consequence is considered to be satisfactory, when KGE > 0.8. When KGE > 0.9, the results are considered excellent [49].

$$\text{NSE} = 1 - \frac{\sum_{i=1}^{n}(Q_{oi} - Q_{si})^2}{\sum_{i=1}^{n}(Q_{oi} - \mu_{oi})^2} \tag{2}$$

$$R = \frac{\sum_{i=1}^{n}(Q_{oi} - \mu_{oi})(Q_{si} - \mu_{si})}{\sqrt{\left[\sum_{i=1}^{n}(Q_{oi} - \mu_{oi})^2\right]\left[\sum_{i=1}^{n}(Q_{si} - \mu_{si})^2\right]}} \tag{3}$$

$$\text{RE} = \frac{\sum_{i=1}^{n}(Q_{si} - Q_{oi})}{\sum_{i=1}^{n} Q_{oi}} \times 100\% \tag{4}$$

$$\alpha = \frac{\sigma_{si}}{\sigma_{oi}} \tag{5}$$

$$\beta = \frac{\mu_{si}}{\mu_{oi}} \tag{6}$$

$$\text{KGE} = 1 - \sqrt{(\alpha - 1)^2 + (\beta - 1)^2 + (R - 1)^2} \tag{7}$$

where n is the number of measured data, Q_{si} ($m^3\ s^{-1}$) is the value of simulated discharge, Q_{oi} ($m^3\ s^{-1}$) is the value of observed discharge, μ_{si} ($m^3\ s^{-1}$) is the mean value of simulated discharge, and μ_{oi} ($m^3\ s^{-1}$) is the mean value of observed discharge.

2.3. Data Description

Constructing the SWAT model requires basic data such as DEM, land use, soil, topography, meteorology, and hydrology. Since the SWAT model requires all raster data to have a unified projection system and geographical coordinates, the projection coordinate system is transformed into WGS_1984_UTM_Zone_51N, and the geographical coordinate system is transformed into GCS_WGS _1984.

2.3.1. Topographic, Soil, and Land Use Data

The DEM data is obtained from the Geospatial Data Cloud, and its spatial resolution is 90 m. The land use data with resolution of 1 km is from the Resources and Environment Science and Data Center. In this study, we used land use data of 1990 and 2010. The soil data is derived from the Harmonized World Soil Database. The resolution of the data is 1 km. The data source used in China is 1:1 million, and the soil data are provided by the second National Land Survey in Nanjing.

2.3.2. Hydro-Meteorological Data

The meteorological data are derived from the daily climatic dataset of the Jiangsu International Ground Exchange station supplied by the National Earth System Science and

Data Center. The maximum and minimum temperature data used in this study is 55 years of daily data from the Nanjing Meteorological Station from 1961 to 2015. The relative humidity, wind speed, and sunshine duration are generated by the weather generator of the SWAT model. The precipitation data are derived from seven rainfall stations in the basin (Aiyuan, Dongshan (Daluo Village), Qianhan Village, Tuqiao, Wudingmen Sluice, Nanjing, and Zhaocun Reservoir stations) from 1978 to 2015. The hydrological data are based on the daily observed discharge data of the Wudingmen Sluice and the Qinhuai River New Sluice, which controlled the drainage source areas of the Qinhuai River Basin from 1978 to 2015.

2.4. GCMs and Climate Change Scenario

The general circulation model has been considered as a direct and effective method to assess the process of global climate change. The CMIP Program aims at better analyzing past, present, and future climate change, and it has been released to the sixth edition, which has not only ushered in a new era for climate science research but has also become a key element of national climate change assessments. The CMIP6 model is affected by factors such as the mechanism, the setting of initial conditions, the resolution, etc., resulting in the different accuracy characteristics of the simulation ability of the same basin and region. According to the applicability of CMIP6 in China, six GCMs projections of BCCCSM2-MR, MRI-ESM2-0, GFDL-ESM4, CanESM5, INM-CM5-0, and MIROC6 were used in this study [27–29]. The downscaled GCMs projections under the three emission scenarios of SSP1-2.6, SSP2-4.5, and SSP5-8.5 are from China Meteorological Administration (CMA). The spatial resolution of each mode is different. The name and basic information of the mode are shown in Table 1.

Table 1. The details of 5 GCMs used in CMIP6.

ID	Name of GCM	Country	Institution	Atmospheric Resolution (Lat × Lon)
1	BCCCSM2-MR	China	BCC	1.125° × 1.125°
2	MRI-ESM2-0	Japan	MRI	1.125° × 1.125°
3	GFDL-ESM4	America	NOAA GFDL	1° × 1.25°
4	CanESM5	Canada	CCCMA	2.7673° × 2.8125°
5	INM-CM5-0	Russia	INM	1.5° × 2°
6	MIROC6	Japan	MIROC	1.389° × 1.406°

The Sixth Assessment Report (AR6) of the Intergovernmental Panel on Climate Change (IPCC), released in 2021, uses the new climate model in CMIP6, in which the new emission scenario driven by different socio-economic models, the shared socioeconomic pathways (SSPs), replaces the representative concentration pathways (RCPs) in CMIP5. As an important part of the new generation of climate change scenarios, SSPs look at five different development models of future economic and social system development, reflecting the relationship between radiation forcing and socioeconomic development. If SSPs are set from the perspective of mitigation and adaptation challenges faced by the future social economy, they can be divided into five paths. The SSP1 scenario describes a world with sustainable development and low climate change challenges. The SSP2 scenario looks at a middle of the road world, that is, social, economic, and technological trends do not deviate significantly from historical patterns and face moderate climate change challenges. The SSP3 scenario presents the worst development direction that society must avoid or prepare to deal with. The SSP4 scenario involves intra-regional and external inequality, with low challenges to be mitigated but large challenges to be adapted. The SSP5 features a high-speed development pattern promoted at the cost of a large amount of fossil fuels. The difference between SSPs and RCPs is that although the radiative forcing predicted by the new scenario in CMIP6 is similar to that in CMIP5, the emission paths and mixed emission paths of carbon dioxide and non-carbon dioxide are different. The three climate scenarios SSP1-2.6, SSP2-4.5, and SSP5-8.5 selected in this study are all upgraded from

RCP2.6, RCP4.5, and RCP8.5, which is an important improvement in CMIP6 scenarios. The SSP1-2.6 scenario in the CMIP6 is low-force, representing the combined effects of low social vulnerability, low mitigation pressure, and low radiative forcing. The SSP2-4.5 scenario is intermediate, representing a combination of medium social vulnerability and medium radiation coercion. The SSP5-8.5 scenario is high-force, representing the combination of high social vulnerability and high radiative forcing, and it is the only path to achieve the man-made radiative forcing level of 8.5 W m^{-2} by 2100.

3. Results and Discussion

3.1. Parameter Sensitivity Analysis

The SUFI-2 algorithm in SWAT-CUP is a reverse method to verify applicability of hydrological model and can analyze the sensitivity of model parameters. There are tens of parameters in the SWAT model. Based on the literature [50–53], 13 of the most sensitive parameters were identified by SWAT-CUP and were listed in Table 2. The model parameters were optimized by using the SUFI-2 algorithm in which a simulations approach was used for best fit by multiple iterations. We use the T-Stat value and *p*-value produced in the SUFI-2 algorithm to evaluate the sensitivity of the model parameters. A higher absolute value of T-Stat indicates a higher sensitivity of the parameters. The *p*-value reflects the significance of the sensitivity. When a *p*-value approaches 0, this indicates the higher significance of the sensitivity. The physical meanings of model parameters were given in Table 2, and the initial ranges of model parameters were given as well based on the previous studies [50–54].

Table 2. The sensitive parameters for discharge with their ranges and fitted values.

Rank	Parameters	Description	T-Stat	*p*-Value	Fitted Value	Range
1	V_ESCO.hru	Soil evaporation compensation factor	−20.847	0.000	0.892	0.8 to 1
2	V_CH_N2.rte	Manning's *n* value for the main channel	−4.684	0.000	0.198	0 to 0.3
3	V_SLSUBBSN.hru	Average slope length	−3.899	0.000	50.180	10 to 150
4	V_GW_DELAY.gw	Groundwater delay	−1.823	0.069	160.620	30 to 450
5	V_ALPHA_BF.gw	Base flow alpha factor	−1.799	0.073	0.623	0 to 1
6	V_SMFMX.bsn	Melt factor for snow on June 21	−1.768	0.078	1.060	0 to 20
7	V_CH_K2.rte	Effective hydraulic conductivity in the main channel	−1.569	0.117	13.625	5 to 130
8	V_GWQMN.gw	Threshold depth of water in shallow aquifer for return flow to occur	−1.566	0.118	1.026	0 to 2
9	V_SMTMP.bsn	Snow melt base temperature	−1.539	0.125	−16.120	−20 to 20
10	R_SOL_K (1).sol	Soil saturated hydraulic conductivity of the first layer	1.455	0.146	0.590	−0.8 to 0.8
11	R_SOL_AWC (1).sol	Soil available water storage capacity of the first layer	−0.991	0.322	−0.057	−0.2 to 0.4
12	V_GW_REVAP.gw	Groundwater reevaporation coefficient	−0.615	0.539	0.181	0 to 0.2
13	R_CN2.mgt	SCS runoff curve number	−0.561	0.575	−0.167	−0.2 to 0.2

Table 2 indicates that the soil evaporation compensation factor (ESCO) is the most sensitive parameter. ESCO mainly dominates the evaporation from soil water. The evaporation of soil water will decrease when ESCO increases. As a result, runoff will increase. The Mannin's *n* coefficient for the main channel (CH_N2) and average slope length (SLSUBBSN) rank No.2 and No.3 in sensitivity of model parameters. SLSUBBSN mainly reflects the influence of the topography and geomorphology on the runoff yield. Based on the value of T-Stat, it can be found that changes in ESCO, CH_N2, and SLSUBBSN have a higher influence on the runoff generation for the Qinhuai River Basin, while the other 10 parameters have a relative lower influence on the runoff yield.

3.2. Applicability Analysis of SWAT Model

We use data series from 1978–2015 to calibrate and validate the SWAT model. In order to eliminate the initial value of the state variable, we take the first two years as a warm-up period. 1980–2000 and 2001–2015 are calibration and validation periods, respectively. Due to land use change, we therefore used land use data of 1990 to represent land use condition in 1980–2000 for model calibration and land use data in 2010 to represent land use condition in 2001–2015 for model validation. Based on the sensitivity analysis of model parameters and the optimal parameters, the daily discharges from 1980–2015 were simulated. We integrated daily discharge to monthly simulated discharge. The applicability of the SWAT model was evaluated with four evaluation indices (NSE, R, RE, and KGE) and flow duration curves (FDC) based on simulations at daily and monthly scales. Figure 4 shows the simulated and observed daily discharge for two typical years of 2000 in the calibration period and 2010 in the validation period. The flow duration curves of the simulated and observed daily discharge for the entire period from 1980–2015 are shown in Figure 5. It can be seen from Figure 4 that the simulated and observed daily discharge fit well for most cases. Although there are some peak discharges being overestimated or underestimated, the relative errors and absolute errors are acceptable according to the Standard for Hydrological Information and Hydrological Forecasting issued by Ministry of Water Resources in 2008 [55]. The flow duration curve in Figure 5 indicates that most high flows (approximately >100 m^3/s) were under-simulated. There are low flows being over- and under-simulated.

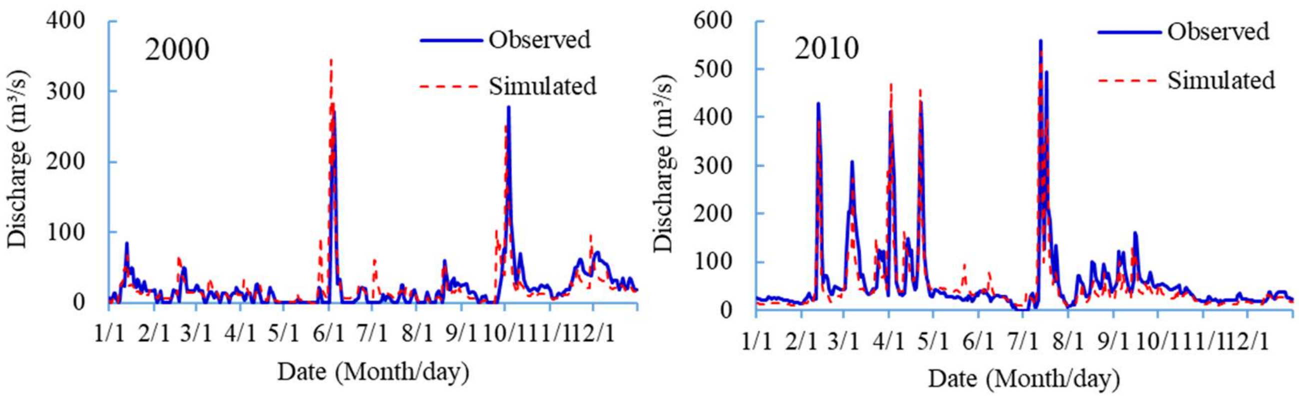

Figure 4. The daily simulated and observed discharges for the typical years (a and b indicate 2000 and 2010).

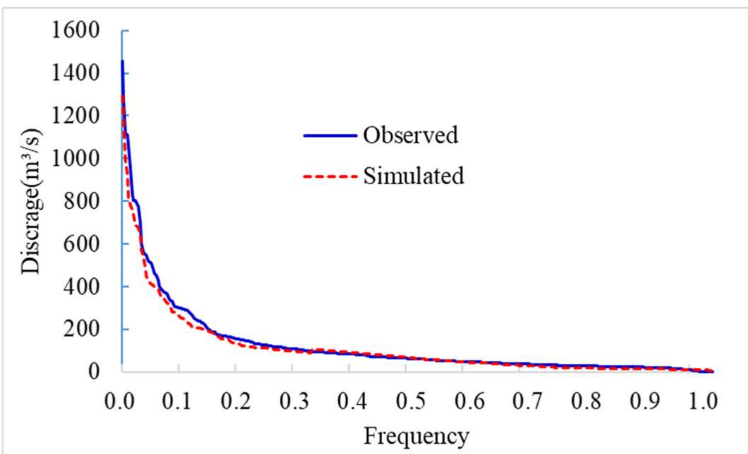

Figure 5. The daily flow duration curves of the catchment.

The simulated and observed monthly discharges in calibration and validation periods were given in Figure 6. The seasonal patterns of the multiple-year average of the simulated and observed discharge are given in Figure 7. The statistical results of SWAT model performance for daily and monthly discharge simulated were summarized in Table 3. Both Figures 6 and 7 show that the simulated and observed monthly discharges match well. The results in Table 3 indicate that the NSE values in calibration and validation periods are above 0.75 for daily discharge simulation, while the corresponding R values are 0.88 and 0.90 for both the periods, respectively. Relatively, the SWAT model performs better for monthly discharge simulation with NSE values, R values, and KGE values, which are much higher than that of daily discharge simulation. Meanwhile, relative errors in calibration and validation periods are ±3.5%. According to the Standard for Hydrological Information and Hydrological Forecasting, the SWAT model reaches to class A (NSE > 0.75) for both daily and monthly discharge simulation.

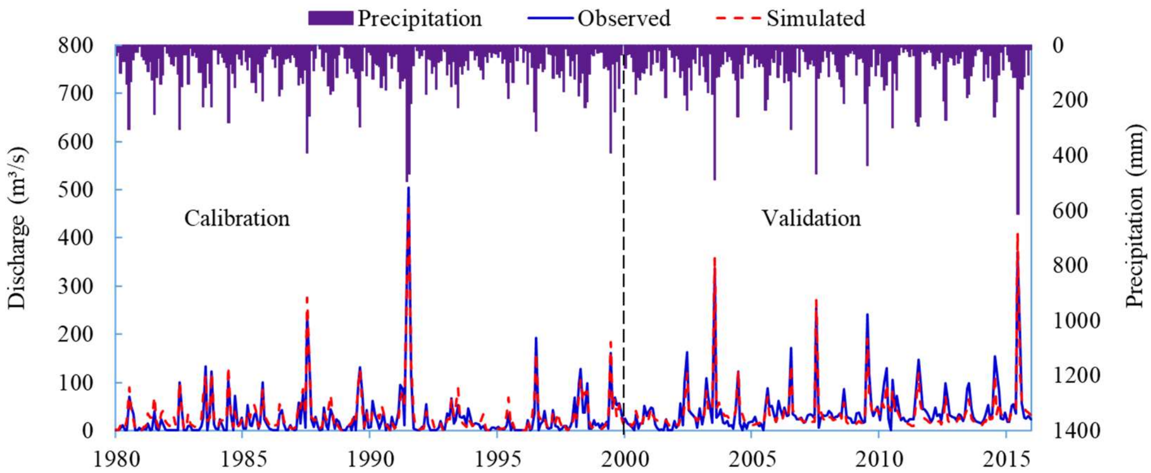

Figure 6. Comparisons between observed and simulated monthly discharge for the calibration period and validation period.

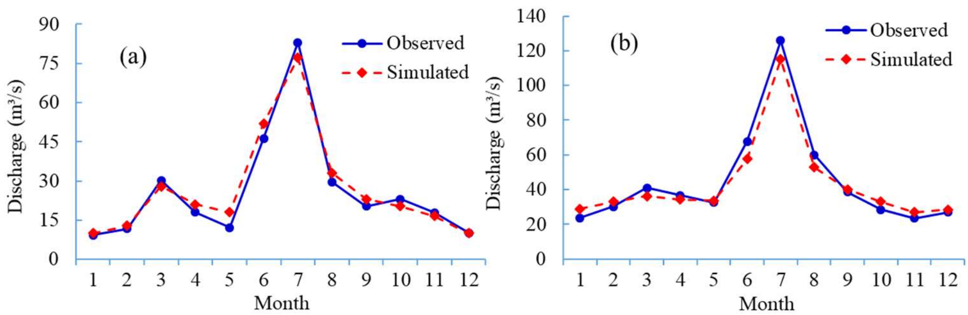

Figure 7. A comparison between the observed and simulated multi-year average monthly discharge in the calibration (**a**) and validation (**b**) periods.

Table 3. The calibration and validation results of the SWAT model.

Temporal Scale	Period	NSE	R	RE	KGE
Daily	Calibration	0.79	0.88	2.30%	0.85
	Validation	0.75	0.90	−3.14%	0.79
Monthly	Calibration	0.87	0.91	2.30%	0.87
	Validation	0.85	0.95	−3.14%	0.83

3.3. Projected Changes in Precipitation and Temperature

Rainfall variability is one of the manifestations of climate change and has a direct impact on the runoff process and the hydrological cycle [56]. The forecast period of the study is from 2025 to 2060, and the baseline period is from 1980 to 2015. The average annual precipitation in the baseline period is 1103.79 mm. Figure 8 shows that under the three emission scenarios of SSP1-2.6, SSP2-4.5, and SSP5-8.5, the average annual precipitation in 2025–2060 has different ranges of increase compared with the baseline period. Generally, predictions of precipitation have great uncertainty. For the SSP1-2.6 emission scenario, most of the GCM projections show a 5.64% precipitation increase in the future on average, with a range of (−3.63%, 15.37%). For the SSP2-4.5 emission scenario, more than half of the GCMs project that precipitation will increase by 2.60% (−0.35%, 4.94%) in the future 2025–2060. For the SSP5-8.5 emission scenario, all GCMs project that precipitation will increase by 6.67% with a range of (1.61%, 12.75%). On average, the average annual precipitation in the Qinhuai River Basin under each SSP scenario changes little and shows an increasing trend (Figure 9). The precipitation increase rate under the SSP1-2.6 emission scenario is the fastest, at 3.86 mm/(10 years). In addition, the precipitation increase rate under other emission scenarios is slower than that in history, and the increasing trend in precipitation under the SSP2-4.5 emission scenario is the slowest, at 1.99 mm/(10 years). The precipitation increase trend under the SSP5-8.5 emission scenario is between the other two emission scenarios.

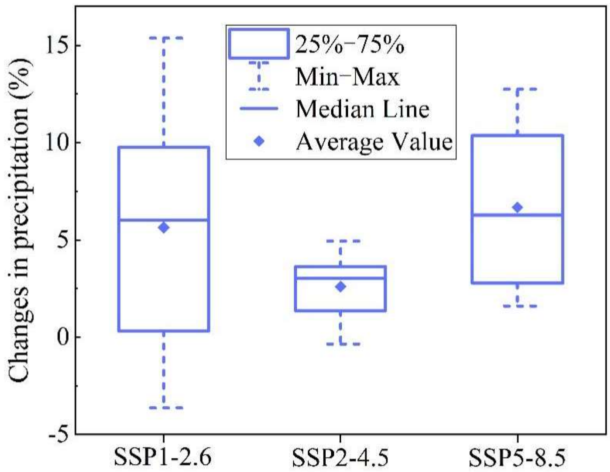

Figure 8. The box−plot of precipitation changes in 6 GCMs relative to the baseline period under the SSP1-2.6, SSP2-4.5, and SSP5-8.5 climate scenarios.

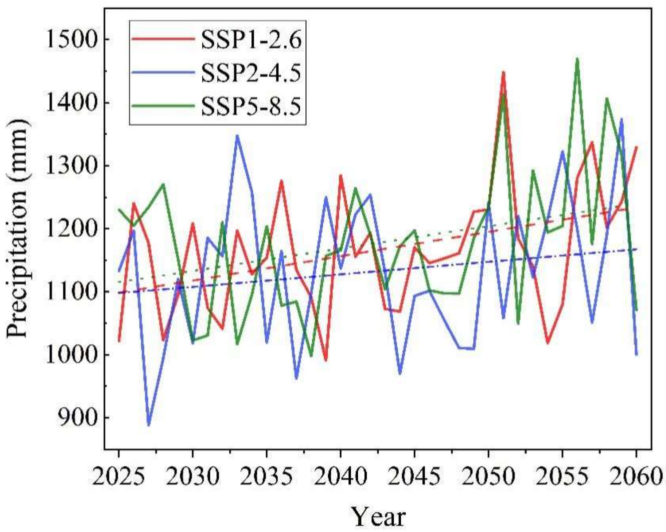

Figure 9. The variation of the precipitation at annual scale in the future period of 2025–2060.

Temperature can indirectly influence the change of runoff through surface evapotranspiration [57]. According to the data of IPCC, there is high confidence that the global mean evaporation increases with global warming, with evaporation increasing by 1–3% for every 1 °C increase in temperature [58]. The multi-year average of maximum and minimum air temperature in the baseline period is 20.63 °C and 12.19 °C, respectively. The changes in the multi-year average maximum and minimum air temperature in the future 2025–2060 relative to the baseline period for the three SSPs emission scenarios were investigated (Figure 10). In the future, the multi-year average temperature in the Qinhuai River Basin will be accompanied by a rapid warming trend and will be higher than that in history as a whole. This may be due to the intensification of global warming caused by the continuous increase in global greenhouse gas emissions, which is reflected in the increasing rate of warming as the equivalent of carbon dioxide emissions increases. Figure 8 indicates that all six GCMs predict that maximum and minimum air temperatures will continue to rise in varying degrees in the future. The maximum air temperature will rise by 1.6 °C (1.26 °C, 2.01 °C), 1.65 °C (1.04 °C, 2.32 °C), and 2.08 °C (1.40 °C, 2.92 °C) under the three emission scenarios of SSP1-2.6, SSP2-4.5, and SSP5-8.5, respectively. The minimum air temperature would rise by 1.40 °C, 1.60 °C, and 1.99 °C, respectively, with ranges of (1.06 °C, 2.01 °C), (1.12 °C, 2.40 °C), and (1.41 °C, 3.00 °C) for the three SSPs scenarios. Based on the precipitation and temperature data, this shows that the hydrothermal conditions in the Qinhuai River Basin will still show warm and humid trends in the future.

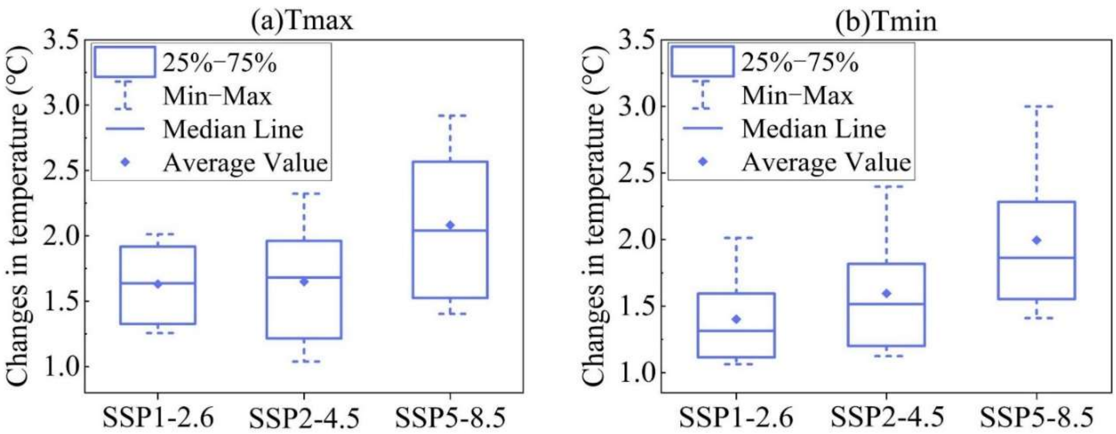

Figure 10. A box−plot of temperature changes of 6 GCMs in (**a**) Tmax, and (**b**) Tmin relative to baseline period under SSP1-2.6, SSP2-4.5, and SSP5-8.5 climate scenarios.

3.4. Climate Change Impact on Runoff

The runoff variation trend from 2025 to 2060 was analyzed based on the global climate model data of precipitation, maximum temperature, and minimum temperature from 1980 to 2014 after down-scaling and deviation correction, as well as the calibrated SWAT model set in the study area. Figure 11 shows that the six GCMs all project that discharge will increase by 8.84% (2.45%, 13.57%) in the SSP2-4.5 emission scenario and 17.96% (7.40%, 32.46%) in the SSP5-8.5 scenario. For the SSP1-2.6 emission scenario, most of the GCMs project that discharge will increase by 16.24% with a range of −4.17% to 38.60%. Future climate projections via the GCMs are largely uncertain. Given the great non-determinacy between different climate models, we applied the multi-model ensemble of GCM under three different emission scenarios in the study to project the future runoff process. The change in the average runoff at the outlet of the Qinhuai River Basin from 2025 to 2060 is shown in Figure 12. As can be seen, under the SSP1-2.6 emission scenario, the maximum annual runoff is 758.4 $m^3\ s^{-1}$ in 2051, and the minimum one is 307.0 $m^3\ s^{-1}$ in 2039. Under the SSP2-4.5 emission scenario, the runoff is greatest in 2059 and lowest in 2027, which are 663.3 $m^3\ s^{-1}$ and 288.3 $m^3\ s^{-1}$ respectively. Under the SSP5-8.5 emission scenario, the average annual runoff reaches the maximum and minimum values in 2058 and 2031, respectively, with a maximum of 701.4 $m^3\ s^{-1}$ and a minimum of 323.5 $m^3\ s^{-1}$. The trend test of runoff series under the three SSPs scenarios was carried out using the Mann–Kendall method. The Z value obtained under the SSP1-2.6 emission scenario is 3.08, which is much higher than the upper limit of the confidence level of 1.96. The absolute values of Z values obtained under the SSP2-4.5 and SSP5-8.5 emission scenarios are 0.97 and 1.40, respectively, and are all within the confidence level threshold of 1.96. The results show that at the 95% confidence interval, the increasing trend of runoff series in the future of Qinhuai River Basin is remarkable only in the SSP1-2.6 scenario, while the increase in runoff under the other two scenarios is not significant.

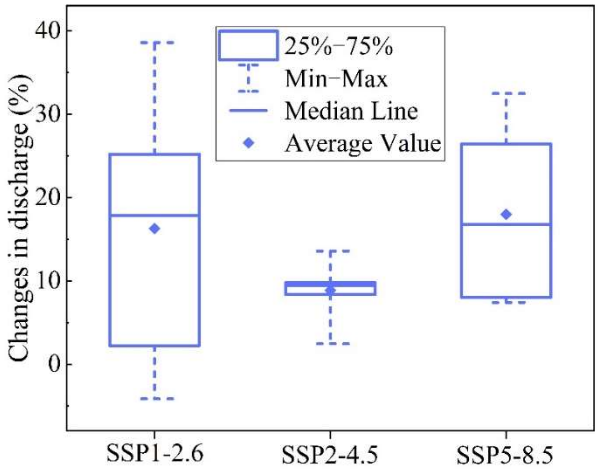

Figure 11. A box−plot of discharge changes in 6 GCMs relative to baseline period under the SSP1-2.6, SSP2-4.5, and SSP5-8.5 emission scenarios.

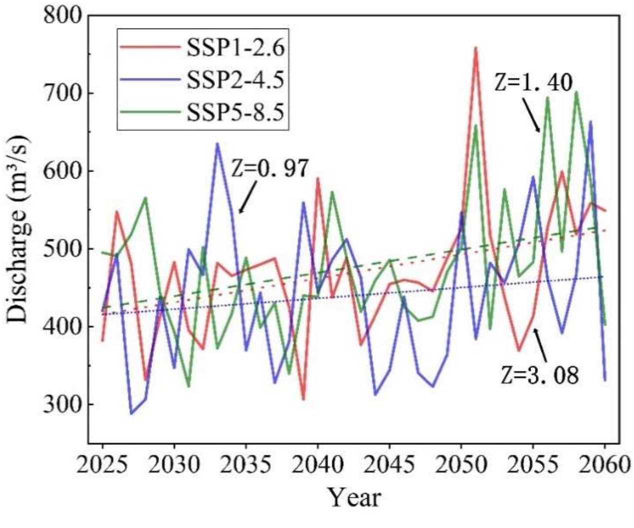

Figure 12. The annual discharge simulated by the calibrated SWAT model for 2025–2060 under the three emission scenarios.

Climate change not only directly affects the hydrological cycle but also affects regional water resources indirectly by changing land use (i.e., vegetation, etc.,). However, the Sankey diagram (Figure 3) shows that land use change in the study catchment is mainly induced by human activities, such as urbanization, changes in agriculture development, etc. This result is consistent with the previous study of Ma et al. (2015) [59]. Climate change contributes a small proportion of land use change. In addition, China is vigorously promoting the protection of cultivated land resources, especially in the 14th Five-Year Plan; the state clearly proposed to take rural agriculture as the key development direction in the future. It can be inferred that the area of cultivated land may not change greatly under the future climate change. We therefore project the future water resources of the catchment by focusing on changes in precipitation and temperature and neglecting the impact of change in land use induced by climate change.

The rise in temperature across the SSPs, with more of an increase in SSP5-8.5 followed by SSP2-4.5 and SSP1-2.6. However, the increase of precipitation and discharge is in the order of SSP5-8.5, SSP1-2.6 and SSP2-4.5. The rise of temperature in SSP2-4.5 scenario is more than that in SSP1-2.6 scenario, while the precipitation and the discharge that is greatly affected by it are higher for SSP1-2.6 and SSP2-4.5, in that order. This might be related to the uncertainty of the results of SSP1-2.6. As we can see in Figures 8 and 11, in the SSP1-2.6 emission scenario, there is a great difference between the high and low values of future runoff, and the evaluation results are quite dispersed, indicating that the results are uncertain, while the evaluation results are relatively concentrated for scenario SSP2-4.5. To some extent, uncertainty in precipitation and temperature forecasts might further affect the hydrological and water resources forecasts of the basin [60,61]. Runoff in the basin always has a certain law of response—linear or non-linear—to the change in precipitation [62]. The change trend of runoff and precipitation in each period in the basin in the future is basically the same. The correlation between precipitation and runoff is good, and the runoff in each scenario increases with the increase of precipitation. This shows that the change in precipitation has a direct impact on the runoff in the basin, and there is a positive correlation between them [40], while the impact of temperature change on runoff is indirect [63]. Previous studies have indicated that the response of runoff to the changes in rainfall is stronger and the precipitation and runoff in the Yangtze River Basin may continue to increase in the future [64–66], which corresponds with the results of this study. Overall, the future runoff of the Qinhuai River Basin may continue to increase, especially in the flood season. This phenomenon will further aggravate the flood control pressure in the wet period, which is not conducive to the future water resources management of Qinhuai River Basin. From the perspective of water resources, local planning departments will face new challenges in the management of water resources in the future. Although the GCMs were used to run the SWAT model, the temporary spatial variability of the runoff process in the basin may be much greater than that of atmospheric process reflected by GCMs. In the process of runoff prediction, there are some uncertainties in the downscaling, climate model, emission scenarios, and hydrological model. Moreover, human activities, such as urban impervious surface expansion, reservoir operations, and other land use changes, also have a significant impact on runoff generation and water resources [67]. However, these aspects are beyond the scope of this study and need further research.

4. Conclusions

The SWAT model performs well for discharge simulation at both daily and monthly scales. The NSE and KGE values of discharge simulation in the calibration and validation periods are above 0.75, and the relative errors (RE) are ±3.5%. The SWAT model is applicable to the Qinhuai River Basin for climate change impact studies.

The projected precipitation and temperature of the Qinhuai River basin will likely increase under the different SSPs scenarios. The average annual precipitation in 2025–2060 under the three SSPs emission scenarios of SSP1-2.6, SSP2-4.5, and SSP5-8.5 will probably increase by 5.64% (−3.63%, 15.37%), 2.60% (−0.35%, 4.94%), and 6.68% (1.61%, 12.75%), respectively, in comparison with the baseline of 1980–2015. The multiple-year average of daily maximum and minimum air temperatures will likely rise by 1.6 °C and 1.4 °C for scenario SSP1-2.6, 1.7 °C, and 1.6 °C for scenario SSP2-4.5, and 2.1 °C and 2.0 °C for scenario SSP5-8.5.

As a result of future climate change, the projected runoff of the Qinhuai River basin shows an increasing trend. The multi-year average runoff in the Qinhuai River Basin was projected to increase by 8.84%–17.96% during 2025–2060 in comparison to the baseline. An increase in runoff will help to relieve the contradiction between the water supply and demand. However, changes in extremes due to rainfall increase might aggravate the flooding situation. Flooding issues induced by climate change will probably be a new challenge to flood control.

Author Contributions: Conceptualization and methodology, J.S.; formal analysis, H.Y. and Z.B.; data curation, H.Y. and G.W.; writing—original draft preparation, J.S.; writing—review and editing, G.W.; and visualization, Z.B. All authors have read and agreed to the published version of the manuscript.

Funding: This research was funded by the National Key Research and Development Programs of China (grant numbers 2017YFA0605002), the National Natural Science Foundation of China (grant numbers 51879162, 41830863), and the Belt and Road Fund on Water and Sustainability of the State Key Laboratory of Hydrology-Water Resources and Hydraulic Engineering (grant numbers 2020nkzd01, 2021490211).

Data Availability Statement: Data is available based on request to corresponding author.

Conflicts of Interest: The authors declare no conflict of interest.

References

1. Pan, Z.K.; Liu, P.; Gao, S.D.; Xia, J.; Chen, J.; Cheng, L. Improving hydrological projection performance under contrasting climatic conditions using spatial coherence through a hierarchical Bayesian regression framework. *Hydrol. Earth Syst. Sci.* **2019**, *23*, 3405–3421. [CrossRef]
2. Yachongtou, B.; Liang, J.; Zeng, G.M.; Li, X.; Lei, M.; Liu, Q. Synergistic effect of land use and climate change on Liuyang River Basin runoff assessed by SWAT model. *J. Water Resour. Water Eng.* **2019**, *30*, 88–94. (In Chinese with an English Abstract) [CrossRef]
3. Qin, D.; Thomas, S.; 259 Authors and TSU (Bern & Beijing). Highlights of the IPCC Working Group I Fifth Assessment Report. *Clim. Change Res.* **2014**, *10*, 1–6. (In Chinese with an English Abstract) [CrossRef]
4. Ahn, K.H.; Merwade, V. Quantifying the relative impact of climate and human activities on streamflow. *J. Hydrol.* **2014**, *515*, 257–266. [CrossRef]
5. Zhang, H.; Zhang, Q.; Liu, Q.; Yan, P. Analysis on variation characteristics and differences of the Climate drying degree between South and North of China. *Plateau Meteorol.* **2016**, *35*, 1339–1351. Available online: https://kns.cnki.net/kcms/detail/detail.aspx?FileName=GYQX201605020&DbName=CJFQ2016 (accessed on 19 July 2021). (In Chinese with an English Abstract)
6. Yin, J.; Gentine, P.; Zhou, S.; Sullivan, S.; Wang, R.; Zhang, Y.; Guo, S. Large increase in global storm runoff extremes driven by climate and anthropogenic changes. *Nat. Commun.* **2018**, *9*, 4389. [CrossRef]
7. Bao, J.; Li, G. Study on Flood Response of Urbanization in Qinhuai River Basin. *Water Resour. Power* **2020**, *38*, 73–77. Available online: https://kns.cnki.net/kcms/detail/detail.aspx?FileName=SDNY202007019&DbName=CJFQ2020 (accessed on 23 July 2021). (In Chinese with an English Abstract)
8. Sun, Y.; Xu, Y.; Gao, B.; Wang, Q.; Li, S. Influence of impervious surface expansion on flood peak under urbanization–A case study of Qinhuai River in Nanjing. *J. Lake Sci.* **2021**, *33*, 1574–1583. (In Chinese with an English Abstract) [CrossRef]
9. Wang, X.; Xie, S.; Du, J.; Cong, D.; Bian, G. Analysis of Spatiotemporal Change of Water Surface and Its Driving Factors in Qinhuai River Basin in Nearly 30 Years. *Remote Sens. Inf.* **2017**, *32*, 34–43. (In Chinese with an English Abstract) [CrossRef]
10. Qin, M.; Hao, L.; Zheng, Q.; Jin, K.; Sun, G. Contributions of Land Use/Cover Change to the Change of Evapotranspiration in Qinhuai River Basin. *Chin. J. Agrometeorol.* **2019**, *40*, 269–283. Available online: https://kns.cnki.net/kcms/detail/detail.aspx?FileName=ZGNY201905001&DbName=CJFQ2019 (accessed on 19 July 2021). (In Chinese with an English Abstract)
11. Yang, H.W.; Chen, X.; Gao, B. Influence of urbanization process on urban waterlogging risk change in Qinhuai River basin. *Jiangsu Water Resour.* **2020**, *10*, 50–57. (In Chinese with an English Abstract) [CrossRef]
12. Gao, Y.; Wang, H.; Lu, X.; Wang, D.; Yuan, Y. Simulation of Rainstorm Flood Response in Qinhuai River Drainage Basin under Land Use Cover Changes. *J. Yangtze River Sci. Res. Inst.* **2018**, *35*, 47–52+66. Available online: https://kns.cnki.net/kcms/detail/detail.aspx?FileName=CJKB201806012&DbName=CJFQ2018 (accessed on 20 July 2021). (In Chinese with an English Abstract)
13. Song, M.; Zhang, J.; Liu, Y.; Wang, G.; Li, C. Evolution and probability distribution of precipitation extreme values in typical urbanized basin in southern China. *J. Hydroelectr. Eng.* **2021**, *40*, 1–13. (In Chinese with an English Abstract) [CrossRef]
14. He, Z.; Shi, L.; Ma, X. Climate change impact analysis and prediction of runoff characteristics of upper Hanjiang River. *Hydro-Sci. Eng.* **2016**, *160*, 37–43. (In Chinese with an English Abstract) [CrossRef]
15. Lin, R.; Fang, G.; Guo, Y.; Wen, X. Analysis of the climate change and runoff response in Duliu River upper basin under the RCP scenarios. *J. Water Resour. Water Eng.* **2017**, *28*, 74–80. Available online: https://kns.cnki.net/kcms/detail/detail.aspx?FileName=XBSZ201701013&DbName=CJFQ2017. (accessed on 19 July 2021). (In Chinese with an English Abstract)
16. Sun, J.; Lu, C.; Ning, Z.; Liu, Y.; Bai, L.; Wang, G. Hydrological characteristics of the Missouri River Basin and its response to changes in meteorological variables. *J. North China Univ. Water Resour. Electr. Power* **2021**, *42*, 20–26. (In Chinese with an English Abstract) [CrossRef]
17. Han, C.; Xi, X.; Zhu, Y. The Impacts of Climate Change and Anthropogenic Activities on the Runoff of Xilamulun River. *J. Irrig. Drain.* **2021**, *40*, 134–140. (In Chinese with an English Abstract) [CrossRef]

18. Li, H. Research on the Streamflow Response to Vegetation Cover Change and Climate Variability. Master's Thesis, Dalian University of Technology, Dalian, China, 2011. Available online: https://kns.cnki.net/KCMS/detail/detail.aspx?dbname=CDFD1214&filename=1012271868.nh (accessed on 23 July 2021). (In Chinese with an English Abstract)
19. Guo, J.; Wang, N.; Li, X. Response of runoff to climate change in upstream generation area of Shiyang River basin. *J. Northwest A F Univ.* **2016**, *44*, 211–218. (In Chinese with an English Abstract) [CrossRef]
20. Sheng, F.; Liu, S.; Liu, Z.; Ye, J.; Yang, M. Comparative analysis on contribution rate to runoff change based on three methods: Case of Pengchongjian small watershed. *Yangtze River* **2021**, *52*, 66–69+75. (In Chinese with an English Abstract) [CrossRef]
21. Kroch, S.A.; Pomeroy, J.W.; Marsh, P. Diagnosis of the hydrology of a small Arctic basin at the tundra−taiga transition using a physically based hydrological model. *J. Hydrol.* **2017**, *550*, 685–703. [CrossRef]
22. Guo, J.; Zhang, Z.; Wang, S.; Strauss, p.; Yao, A. Appling SWAT model to explore the impact of changes in land use and climate on the streamflow in a Watershed of Northern China. *Acta Ecol. Sin.* **2014**, *34*, 1559–1567. (In Chinese with an English Abstract) [CrossRef]
23. Wang, Z.; Liu, C.; Huang, Y. The Theory of SWAT Model and its Application in Heihe Basin. *Prog. Geogr.* **2003**, *22*, 79–86. (In Chinese with an English Abstract) [CrossRef]
24. Li, R.; Huang, H.; Yu, G.; Yu, H. Contributions of climatic variation and human activities to streamflow changes in the Lancang−Mekong River Basin. *Resour. Sci.* **2021**, *43*, 2428–2441. [CrossRef]
25. Zhang, A.; Wang, S.; Wang, P.; Shang, Z. Runoff Simulation of Zishui Basin Based on SWAT Model. *J. China Hydrol.* **2017**, *37*, 38–42+26. Available online: https://kns.cnki.net/kcms/detail/detail.aspx?FileName=SWZZ201705007&DbName=CJFQ2017 (accessed on 24 July 2021). (In Chinese with an English Abstract)
26. Piniewski, M.; Szcześniak, M.; Kardel, I.; Berezowski, T.; Okruszko, T.; Srinivasan, R.; Vikhamar Schuler, D.; Kundzewicz, Z.W. Hydrological modelling of the Vistula and Odra river basins using SWAT. *Hydrol. Sci. J.* **2017**, *62*, 1266–1289. [CrossRef]
27. Zhu, H.; Jiang, Z.; Li, J.; Li, W.; Sun, C.; Li, L. Does CMIP6 Inspire More Confidence in Simulating Climate Extremes over China? *Adv. Atmos. Sci.* **2020**, *37*, 1119–1132. [CrossRef]
28. Zhang, J.; Lun, Y.; Liu, L.; Liu, Y.; Li, X.; Xu, Z. CMIP6 evaluation and projection of climate change in Tibetan Plateau. *J. Beijing Norm. Univ. (Nat. Sci.)* **2022**, *58*, 77–89. (In Chinese with an English Abstract) [CrossRef]
29. Zhang, L.; Chen, X.; Xin, X. Short commentary on CMIP6 Scenario Model Intercomparison Project (ScenarioMIP). *Clim. Chang. Res.* **2019**, *15*, 519–525. (In Chinese with an English Abstract) [CrossRef]
30. Yan, J.; Wu, B.; He, Q. An anisotropic IDW interpolation method with multiple parameters cooperative optimization. *Acta Geod. Et Cartogr. Sin.* **2021**, *50*, 675–684. Available online: https://kns.cnki.net/kcms/detail/detail.aspx?FileName=CHXB202105012&DbName=CJFQ2021 (accessed on 24 July 2021). (In Chinese with an English Abstract)
31. Chen, J.; Brissette, F.P.; Chaumont, D.; Braun, M. Performance and uncertainty evaluation of empirical downscaling methods in quantifying the climate change impacts on hydrology over two North American river basins. *J. Hydrol.* **2013**, *479*, 200–214. [CrossRef]
32. Tobler, W.R. A computer movie simulating urban growth in the detroit region. *Econ. Geogr.* **1970**, *46*, 234–240. [CrossRef]
33. Yi, G.; Zhang, T.; He, Y.; Ye, H.; Li, J.; Bie, X.; Liu, D. Applicability analysis of four spatial interpolation methods for air temperature. *J. Chengdu Univ. Technol. (Sci. Technol. Ed.)* **2020**, *47*, 115–128. (In Chinese with an English Abstract) [CrossRef]
34. Chen, J.; Brissette, F.P.; Chaumont, D.; Braun, M. Finding appropriate bias correction methods in downscaling precipitation for hydrologic impact studies over North America. *Water Resour. Res.* **2013**, *49*, 4187–4205. [CrossRef]
35. Gu, L.; Yin, J.; Zhang, H.; Wang, H.; Yang, G.; Wu, X. On future flood magnitudes and estimation uncertainty across 151 catchments in mainland China. *Int. J. Climatol.* **2020**, *41*, E779–E800. [CrossRef]
36. Zhuan, M.; Chen, J.; Shen, M.; Xu, C.; Chen, H.; Xiong, L. Timing of human−induced climate change emergence from internal climate variability for hydrological impact studies. *Hydrol. Res.* **2018**, *49*, 421–437. [CrossRef]
37. He, X.; Meng, J.; Guo, H.; Tian, Z. Effect of Land Use and Climate Change on Runoff in Luohe River Basin. *Water Resour. Power* **2021**, *39*, 31–34. Available online: https://kns.cnki.net/kcms/detail/detail.aspx?FileName=SDNY202110008&DbName=DKFX2021 (accessed on 24 July 2021). (In Chinese with an English Abstract)
38. Celina, A.; Patricia, J.S.; Adrián, L.B.; Pacheco, J.P.; Javier, S.A. Analysing the Impact of Climate Change on Hydrological Ecosystem Services in Laguna del Sauce (Uruguay) Using the SWAT Model and Remote Sensing Data. *Remote Sens.* **2021**, *13*, 2014. [CrossRef]
39. Zhao, A.; Liu, X.; Zhu, X.; Pan, Y.; Li, Y. Spatiotemporal patterns of droughts based on SWAT model for the Weihe River Basin. *Prog. Geogr.* **2015**, *34*, 1156–1166. Available online: https://kns.cnki.net/kcms/detail/11.3858.p.20150924.1038.016.html (accessed on 25 July 2021). (In Chinese with an English Abstract)
40. Tian, J.; Guo, S.; Liu, D.; Chen, Q.; Wang, Q.; Yin, J.; Wu, X.; He, S. Impacts of climate and land use/cover changes on runoff in the Hanjiang River basin. *Acta Geogr. Sin.* **2020**, *75*, 2307–2318. Available online: https://kns.cnki.net/kcms/detail/detail.aspx?FileName=DLXB202011004&DbName=DKFX2020 (accessed on 25 July 2021). (In Chinese with an English Abstract)
41. Cheng, C. Impacts of land use /land cover change and climate change on the runoff in Yuan River basin based on SWAT model. *Sci. Soil Water Conserv.* **2020**, *18*, 52–59. (In Chinese with an English Abstract) [CrossRef]
42. Arnold, J.G.; Srinivasan, R.; Muttiah, R.S.; Williams, J.R. LARGE area hydrologic modeling and assessment part I: Model development. *J. Am. Water Resour. Assoc.* **1998**, *34*, 73–89. [CrossRef]

43. Tian, Y.; Wang, Z.; Zhang, X. Development and Advances in Application of SWAT Model. *J. Anhui Agri. Sci.* **2012**, *40*, 3480–3483+3486. (In Chinese with an English Abstract) [CrossRef]
44. Liu, H. Progress of Study and Application of SWAT Model. *Subtrop. Soil Water Conserv.* **2019**, *31*, 34–37. Available online: https://kns.cnki.net/kcms/detail/detail.aspx?FileName=FJSB201902008&DbName=CJFQ2019. (accessed on 25 July 2021). (In Chinese with an English Abstract)
45. Osei, M.A.; Amekudzi, A.L.; Wemegah, D.D.; Preko, K.; Gyawu, E.S.; Obiri-Danso, K. The impact of climate and land−use changes on the hydrological processes of Owabi catchment from SWAT analysis. *J. Hydrol. Reg. Stud.* **2019**, *25*, 100620. [CrossRef]
46. Nilawar, A.P.; Waikar, M.L. Impacts of climate change on streamflow and sediment concentration under RCP 4.5 and 8.5: A case study in Purna river basin, India. *Sci. Total Environ.* **2019**, *650*, 2685–2696. [CrossRef]
47. Li, C.; Fang, H. Assessment of climate change impacts on the streamflow for the Mun River in the Mekong Basin, Southeast Asia: Using SWAT model. *Catena* **2021**, *201*, 105199. [CrossRef]
48. Gupta, H.V.; Kling, H.; Yilmaz, K.K.; Martinez, F.G. Decomposition of the mean squared error and NSE performance criteria: Implications for improving hydrological modeling. *J. Hydrol.* **2009**, *377*, 80–91. [CrossRef]
49. Feng, C.; Mao, D.; Zhou, H.; Cao, Y.; Hu, G. Impacts of climate and land use changes on runoff in the Lianshui basin. *J. Glaciol. Geocryol.* **2017**, *39*, 395–406. Available online: https://kns.cnki.net/kcms/detail/detail.aspx?FileName=BCDT201702020&DbName=CJFQ2017 (accessed on 25 July 2021). (In Chinese with an English Abstract)
50. Lin, B.; Chen, Y.; Chen, X. A Study on Regional Difference of Hydrological Parameters of SWAT Model. *J. Nat. Resour.* **2013**, *28*, 1988–1999. (In Chinese with an English Abstract) [CrossRef]
51. Wu, J.; Zheng, H.; Xi, Y. SWAT-Based Runoff Simulation and Runoff Responses to Climate Change in the Headwaters of the Yellow River, China. *Atmosphere* **2019**, *10*, 509. [CrossRef]
52. Haider, H.; Zaman, M.; Liu, S.; Saifullah, M.; Usman, M.; Chauhdary, J.N.; Anjum, M.N.; Waseem, M. Appraisal of Climate Change and Its Impact on Water Resources of Pakistan: A Case Study of Mangla Watershed. *Atmosphere* **2020**, *11*, 1071. [CrossRef]
53. Tuo, Y.; Duan, Z.; Disse, M.; Chiogna, G. Evaluation of precipitation input for SWAT modeling in Alpine catchment: A case study in the Adige river basin (Italy). *Sci. Total Environ.* **2016**, *573*, 66–82. [CrossRef] [PubMed]
54. Abbaspour, K.C. *SWAT−CUP 2012: SWAT Calibration and Uncertainty Programs–A User Manual*; Swiss Federal Institute of Aquatic Science and Technology: Dübendorf, Switzerland, 2014.
55. *GB/T 22482−2008*; Standard for Hydrological Information and Hydrological Forecasting. Ministry of Water Resources: Beijing, China, 2008. (In Chinese)
56. Choi, W.; Nauth, K.; Choi, J.; Becker, S. Urbanization and Rainfall−Runoff Relationships in the Milwaukee River Basin. *Prof. Geogr.* **2016**, *68*, 14–25. [CrossRef]
57. Mei, J.; Tang, Y.; Li, Y.; Liu, Y.; Jiang, Q.; Chen, X. Simulation of the Hydrological Response of Xunhe River Basin to Climate Change Using the SWAT model. *J. Hydroecology* **2021**, *42*, 7–13. [CrossRef]
58. IPCC. *Climate Change 2021: The Physical Science Basis*; Cambridge University Press: Cambridge, UK; New York, NY, USA, 2021.
59. Ma, X.; Bian, Z.; Li, N.; Li, Y.; Zhao, J.; Zeng, C.; Wang, L. Land Use Change and Its Driving Mechanism in Qinhuai River Watershed During 1980–2010. *Bull. Soil Water Conserv.* **2015**, *35*, 272–276. (In Chinese with an English Abstract) [CrossRef]
60. Minville, M.; Brissette, F.; Leconte, R. Uncertainty of the impact of climate change on the hydrology of a nordic watershed. *J. Hydrol.* **2008**, *358*, 70–83. [CrossRef]
61. Ahmadalipour, A.; Moradkhani, H.; Rana, A. Accounting for downscaling and model uncertainty in fine−resolution seasonal climate projections over the Columbia River Basin. *Clim. Dyn.* **2018**, *50*, 717–733. [CrossRef]
62. Zhang, C.; Bao, Z.; Yang, X.; Liu, Z.; Guan, X.; Wang, G.; Liu, C. Research on the influence of climate change and land use change on hydrological process. *J. North China Univ. Water Resour. Electr. Power (Nat. Sci. Ed.)* **2019**, *40*, 46–50. (In Chinese with an English Abstract) [CrossRef]
63. Yan, Y.; Xue, B.; Zhang, L. Impact of land use and climate change on runoff in the upper reaches of Hailaer River based on SWAT model. *J. Liaocheng Univ. (Nat. Sci. Ed.)* **2020**, *33*, 89–96. (In Chinese with an English Abstract) [CrossRef]
64. Qiao, C.; Ning, Z.; Wang, Y.; Sun, J.; Lin, Q.; Wang, G. Impact of Climate Change on Water Availability in Water Source Areas of the South-to-North Water Diversion Project in China. *Front. Earth Sci.* **2021**, *9*, 747429. [CrossRef]
65. Bian, H.; Lü, H.; Sadeghi, A.; Zhu, Y.; Yu, Z.; Ouyang, F.; Su, J.; Chen, R. Assessment on the Effect of Climate Change on Streamflow in the Source Region of the Yangtze River, China. *Water* **2017**, *9*, 70. [CrossRef]
66. Lu, W.; Wang, W.; Shao, Q.; Yu, Z.; Hao, Z.; Xing, W.; Yong, B.; Li, J. Hydrological Projections of Future Climate Change Over the Source Region of Yellow River and Yangtze River in the Tibetan Plateau: A Comprehensive Assessment by Coupling RegCM4 and VIC Model. *Hydrol. Process* **2018**, *32*, 2096–2117. [CrossRef]
67. Worku, T.; Khare, D.; Tripathi, S.T. Modeling runoff-sediment response to land use/land cover changes using integrated GIS and SWAT model in the Beressa watershed. *Environ. Earth Sci.* **2017**, *76*, 1–14. [CrossRef]